JACS
JOURNAL OF THE AMERICAN CHEMICAL SOCIETY
Article
pubs.acs.org/JACS

Ferroelectric Polarization and Second Harmonic Generation in Supramolecular Cocrystals with Two Axes of Charge-Transfer

Ashwin Narayanan,[†,a] Dennis Cao,[‡,a] Laszlo Frazer,[§] Alok S. Tayi,[†] Anthea K. Blackburn,[‡] Andrew C.-H. Sue,[‡] John B. Ketterson,[§,∥] J. Fraser Stoddart,[*,‡] and Samuel I. Stupp[*,†,‡,⊥,#]

[†]Department of Materials Science and Engineering, [‡]Department of Chemistry, [§]Department of Physics and Astronomy, [∥]Department of Electrical Engineering and Computer Science, and [⊥]Department of Biomedical Engineering, Northwestern University, Evanston, Illinois 60208, United States

[#]Department of Medicine and Simpson-Querrey Institute for BioNanotechnology, Northwestern University, Chicago, Illinois 60611, United States

Supporting Information

ABSTRACT: Ferroelectricity in organic materials remains a subject of great interest, given its potential impact as lightweight information storage media. Here we report supramolecular charge-transfer cocrystals formed by electron acceptor and donor molecules that exhibit ferroelectric behavior along two distinct crystallographic axes. The solid-state superstructure of the cocrystals reveals that a 2:1 ratio of acceptor to donor molecules assemble into nearly orthogonal mixed stacks in which the molecules are positioned for charge-transfer in face-to-face and edge-to-face orientations, held together by an extended hydrogen-bonding network. Polarization hysteresis was observed along the face-to-face and edge-to-face axes at room temperature. The noncentrosymmetric nature of the cocrystals, required to observe ferroelectric behavior, is demonstrated using second harmonic generation measurements. This finding suggests the possibility of designing supramolecular arrays in which organic molecules support multidimensional information storage.

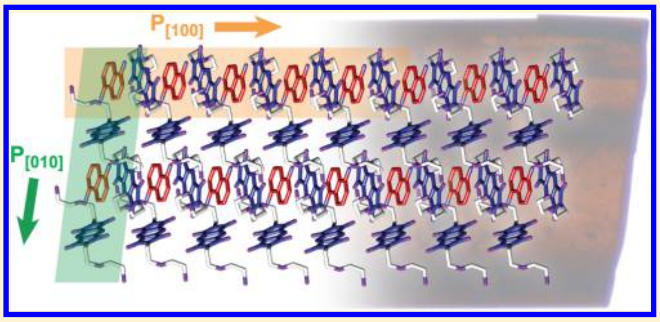

INTRODUCTION

Materials that possess nonlinear optical as well as ferroelectric properties with switchable spontaneous electrical polarization hold great promise in electronic memory and optoelectronic applications.[1,2] Inorganic ferroelectric materials, such as the prototypical BaTiO$_3$, are composed of two ionic sublattices that experience a spontaneous breaking of inversion symmetry by atomic displacement along one direction.[3,4] This property, in turn, gives rise to a nonlinear optical response, characterized by second harmonic generation (SHG).[5,6] Recent breakthroughs in organic crystals, hybrid frameworks, and liquid crystalline materials have drawn attention to organic ferroelectric materials that have performances approaching those of their inorganic counterparts.[7−11]

Mixed-stack charge-transfer (CT) complexes,[12] in which electron donor and acceptor molecules assemble face-to-face in an alternating mixed stack, are promising candidates for ferroelectric organic materials on account of their tunable neutral and ionic ground states.[13] We have developed[14] a motif termed lock-arm supramolecular ordering (LASO) to obtain ordered, close-packed, solvent-free, and robust crystalline materials by leveraging a combination of charge-transfer, $\pi{-}\pi$ stacking, van der Waals, and complementary hydrogen-bonding interactions. In three of the LASO cocrystals, we observed room temperature ferroelectric hysteresis.[8] We hypothesized that the spontaneous polarizations observed at room temperature, rather than solely at cryogenic temperatures, are enabled by the complementary hydrogen bonding and charge-transfer interactions that stabilize the polar, dimerized donor−acceptor supramolecular network. Seeking to probe structure−property relationships in these cocrystals, we obtained a thin sheet-like LASO cocrystal characterized by two crystallographically unique axes, indicative of two preferred directions of crystal growth. Polarized absorption spectra of the cocrystal suggests CT interactions in both the face-to-face and edge-to-face directions.[20]

In this work, we investigate in great detail the CT cocrystal (Figure 1a), incorporating a 2:1 ratio of pyromellitic diimide acceptor **1** to 5-amino-1-naphthol donor **2**. The crystal structure (Figure 1b) of $(\mathbf{1})_2{\cdot}\mathbf{2}$, obtained by single-crystal X-ray diffraction, reveals[14] that each donor molecule engages in (i) face-to-face CT interactions, reminiscent of a conventional mixed-stack CT complex along the [100] crystallographic axis, and (ii) edge-to-face CT interactions with additional acceptor molecules along the [010] direction. In the following discussion, the face-to-face stacking [100] direction will be referred to as the *mixed-stack axis* and the edge-to-face [010]

Received: March 6, 2017
Published: June 29, 2017

DOI: 10.1021/jacs.7b02279
J. Am. Chem. Soc. 2017, 139, 9186−9191

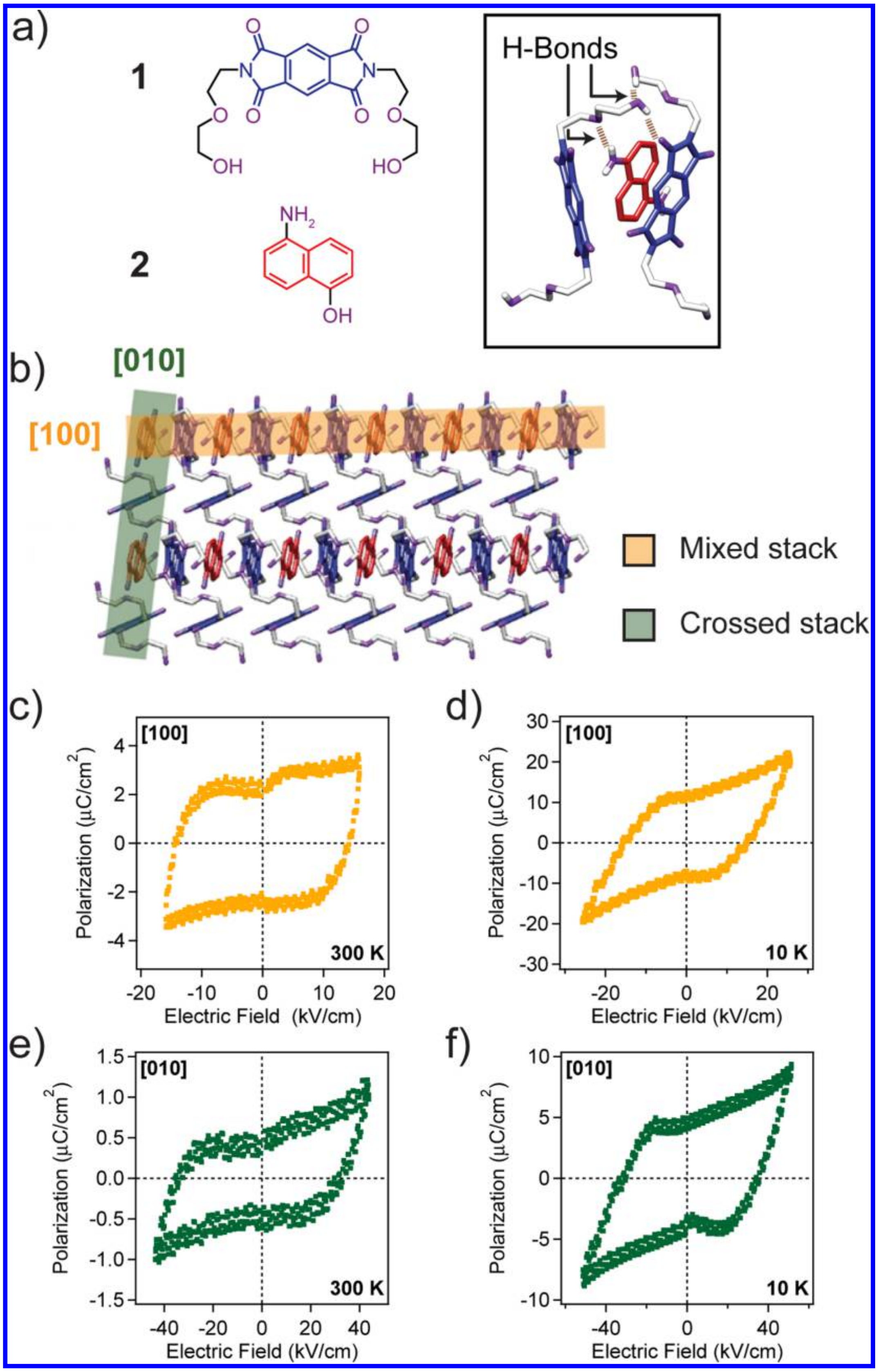

Figure 1. (a) Structural formulas of electron acceptor **1** (blue) and electron donor **2** (red) with hydrogen-bond donors (OH and NH_2) and hydrogen-bond acceptors (C=O and OCH_2CH_2). Crystal structure of $(\mathbf{1})_2\cdot\mathbf{2}$ (inset a). The heteroatoms (purple) that participate in noncovalent bonding interactions as well as the hydrogen bonds (black hatched lines) between atoms are identified. (b) The superstructure of the cocrystal with the mixed-stack and crossed-stack axes; the axes are highlighted in orange and green, respectively. Polarization versus electric-field curves measured along the (c),(d) [100] stack and (e),(f) [010] axes. Polarization hysteresis loops along the [100] axis were observed at (c) 300 K and (d) 10 K, and along the [010] axis at (e) 300 K and (f) 10 K. All hysteresis measurements were performed at $f = 0.1$ Hz.

DOI: 10.1021/jacs.7b02279
J. Am. Chem. Soc. 2017, 139, 9186−9191

stacking direction as the *crossed-stack axis*. Given the nature of the crystal structure, we have explored here the possibility of anisotropic ferroelectric behavior as well as the signatures for noncentrosymmetry using second harmonic microscopy and spectroscopy.

■ RESULTS AND DISCUSSION

The cocrystal $(\mathbf{1})_2\cdot\mathbf{2}$ was grown under ambient conditions by liquid–liquid diffusion of 1-chlorobutane into a 1,2-dichloroethane solution of the two compounds. See Experimental Section and SI. Morphologically, the solvent-free cocrystals grow in two directions to yield thin sheets (Figure S2) that are at times several centimeters in length. Evidence for ferroelectricity in cocrystal $(\mathbf{1})_2\cdot\mathbf{2}$ was obtained along both the mixed-stack and crossed-stack axes (Figure 1b) at 300 and 10 K by measuring (Figure 1c–f) polarization hysteresis curves of electric displacement as a function of the applied electric field. Depolarization fields,[15,16] typically observed in thin-film devices, were assumed to be negligible because the ferroelectric device lengths (Table S3) were on the order of hundreds of micrometers. The mixed-stack axis [100] has a maximum room-temperature polarization ($P_{\max}$) of 3.5 μC/cm^2 and a remnant polarization (P_r) of 2.4 μC/cm^2, whereas the crossed-stack axis [010] has a $P_{\max}$ of 1.1 μC/cm^2 and a P_r of 0.5 μC/cm^2. Lowering the temperature to 10 K allowed us to bias the crystals at higher electric fields and observe curves having larger hysteresis with P_r values of 10 μC/cm^2 and 4.5 μC/cm^2 along the [100] and [010] axes, respectively. Dielectric breakdown of the crystals at high voltages limits the maximum observable polarization, and as a result, the hysteresis curves measured are undersaturated. Joule heating and crystal degradation at high voltages are possible causes for this observed effect.[7] Nonetheless, we found that at both 10 K and room temperature, the polarization curves measured for $(\mathbf{1})_2\cdot\mathbf{2}$ do not resemble the banana loops that are often observed as a false-positive indication of ferroelectricity.[17]

The ferroelectric axes in cocrystal $(\mathbf{1})_2\cdot\mathbf{2}$ are nearly orthogonal (~84°), and, as a consequence, applying a field along any one axis would result in a far smaller projection on the second axis (Figure S3). The parasitic field results in a negligible polarization along the second axis. The unique geometry of the two ferroelectric axes, along with the two observed directions of charge-transfer,[14] suggest that the two polarization states in cocrystal $(\mathbf{1})_2\cdot\mathbf{2}$ are decoupled. This decoupling and asymmetry between the two nonequal ferroelectric polarizations are unique among ferroelectric materials. Ferroelectricity across multiple axes has traditionally been limited to materials that form ferroelectric vortices, or have multiple crystallographically equivalent polarization axes. Ferroelectric vortices are topological defects in ferroelectric materials, characterized by closure domains where adjacent in-plane polarizations align head-to-tail with a domain angle of less than 180°, resulting in a closed polarization loop.[18−21] Although examples of naturally occurring[22] and induced[23] ferroelectric vortices have been reported, the sizes of these vortices are restricted to the nanoscale because of their metastable nature. Ferroelectric materials with multiple crystallographically equivalent axes can also display ferroelectric polarization across multiple axes. One such material is the organic crystal 2-methylbenzimidazole, wherein ferroelectric behavior arises from proton tautomerization.[24] In this compound, tetragonal crystal symmetry allows for ferroelectric polarization of equal magnitude across two crystallographically equivalent axes. What distinguishes the ferroelectric cocrystal reported here from these examples is that cocrystal $(\mathbf{1})_2\cdot\mathbf{2}$ displays anisotropic, single-crystal ferroelectric polarizations across two crystallographically unique axes. We believe this phenomenon can be attributed to the combined effects of charge-transfer along more than one axis and the existence of a three-dimensional hydrogen-bonding network in the donor–acceptor cocrystal.

In an effort to determine the ferroelectric Curie temperature (T_c) of the cocrystal $(\mathbf{1})_2\cdot\mathbf{2}$, we measured (Figure 2) dielectric constants along the two ferroelectric axes as a function of temperature. In both cases, the expected discontinuity, characteristic of a ferroelectric-to-paraelectric phase transition,[4] was not observed within the 7 to 400 K temperature range. This observation suggests that the T_c lies outside the range of this measurement and close to the decomposition temperature of the cocrystal. The lack of an observable Curie temperature is likely the result of the stable hydrogen-bonding network in this system. Other examples[25−28] of ferroelectric materials are known for which a Curie temperature is not observed. One such material is poly(vinylidene fluoride) (PVDF), where the T_c has been estimated by extrapolation from copolymer samples, because PVDF melts before undergoing any ferroelectric-to-paraelectric transition. The frequency dependence of the dielectric constants of cocrystal $(\mathbf{1})_2\cdot\mathbf{2}$ can be attributed to the dynamics of domain-wall motion along the mixed- and crossed-stack axes, a phenomenon not uncommon among mixed-stack charge-transfer complexes.[29,30] This is especially apparent at lower temperatures, where the frequency-dependent dielectric response slows down enough to be observed in the measured frequency ranges.

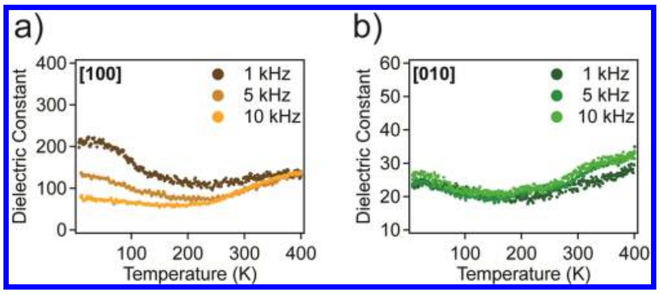

Figure 2. Dielectric constant measurements between 7 and 400 K on cocrystal $(\mathbf{1})_2\cdot\mathbf{2}$ along the (a) mixed-stack [100] and (b) crossed-stack [010] axes. No ferroelectric Curie transition is observed along either axis, which is indicative of a ferroelectric-paraelectric phase transition that is outside the measurement range. All dielectric measurements were performed at 2 V with f = 1, 5, and 10 kHz.

We previously reported the crystal structure of $(\mathbf{1})_2\cdot\mathbf{2}$ to be centrosymmetric.[14] This property is, of course, not consistent with the observed ferroelectric behavior. We compared diffraction data of cocrystal $(\mathbf{1})_2\cdot\mathbf{2}$ collected at (i) cryogenic and (ii) room temperatures, as well as (iii) after the application of electric fields. In all three cases, the crystallographic data for the cocrystals refine (Table S1) to the centrosymmetric space group $P\bar{1}$. Attempts to refine the data in a noncentrosymmetric space group were unsuccessful, and multiple inconsistencies with missing symmetry elements in the data were flagged by *checkCIF*.[31,32] On the basis of the indications of ferroelectric behavior in cocrystal $(\mathbf{1})_2\cdot\mathbf{2}$, we decided to assess the hypothesis that X-ray crystallography alone is unable to resolve the source of noncentrosymmetry in these cocrystals.

DOI: 10.1021/jacs.7b02279
J. Am. Chem. Soc. 2017, 139, 9186−9191

Second harmonic generation is a nonlinear optical effect that is well established as a tool for elucidating structure and detecting noncentrosymmetry in electronic and magnetic crystals.[33−36] Specifically, SHG refers to the process where two photons undergo frequency doubling (wavelength halving) when incident on a material. SHG is distinct from other photoexcitation processes in that it does not require a photoinduced excited state and is unique to materials that lack a crystallographic inversion center. This nonlinear optical phenomenon has been previously demonstrated in organic crystals[37−39] and biological samples[40] as well as in organic ferroelectric materials.[24,41,42] Two-photon confocal microscopy on a single crystal of $(\mathbf{1})_2{\cdot}\mathbf{2}$ under ambient conditions at zero applied field allowed us to image (Figure 3) a second harmonic response. The lack of an inversion center in cocrystal $(\mathbf{1})_2{\cdot}\mathbf{2}$ results in frequency doubling (wavelength halving) of the incident two-photon radiation. Consequently, the cocrystal is only "seen" by the detector that possesses a detection range within half the incident multiphoton wavelength. To delineate this observation from potential photoexcitation processes, the cocrystal was excited at multiple incident wavelengths. Tuning the incident two-photon wavelength from 850 to 950 nm results in the detection of cocrystal $(\mathbf{1})_2{\cdot}\mathbf{2}$ changing from Detector 1 to Detector 2 because the second harmonic wavelength falls beyond the detection limit of Detector 1 and into the detection range of Detector 2. This behavior proves that the detected photons arise solely due to SHG within the cocrystal, suggestive of a noncentrosymmetric crystal structure. The same pattern was observed (Figure S4) with the two-photon confocal microscope in transmission mode, which limits the possibility of surface-mediated SHG.

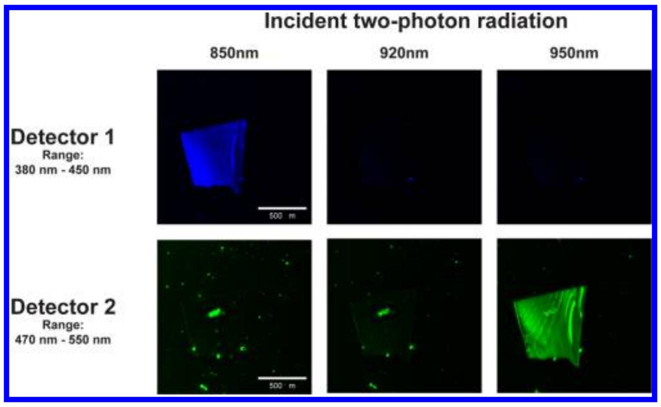

Figure 3. Two-photon confocal microscopy of cocrystal $(\mathbf{1})_2{\cdot}\mathbf{2}$, which can only be detected when the induced second harmonic response falls within the detector range. For example, incident two-photon radiation at 850 nm induced a second harmonic response at 425 nm, which can only be imaged by Detector 1. Tuning the incident radiation screens the detection of cocrystal $(\mathbf{1})_2{\cdot}\mathbf{2}$ based on the wavelength of the second harmonic response.

To further elucidate noncentrosymmetry in cocrystal $(\mathbf{1})_2{\cdot}\mathbf{2}$, we measured the spectroscopic SHG of powdered crystals under ambient conditions at zero applied field. SHG signals were observed (Figure 4) for cocrystal $(\mathbf{1})_2{\cdot}\mathbf{2}$ at second harmonic wavelengths greater than 650 nm, corresponding to the optically transparent region of the cocrystal. This spectroscopic evidence of SHG, combined with the second harmonic images obtained by two-photon confocal microscopy, prove that the cocrystal does indeed have a noncentrosymmetric structure. It is important to note the difference in the detected second harmonic wavelengths using spectroscopic versus microscopic techniques. Using spectroscopy, we only observed SHG at harmonic wavelengths longer than 650 nm, whereas we observed a second harmonic response at 425 nm when using two-photon microscopy. This disparity can be attributed to the absorption of second harmonic photons. Absorption is more important in the powder than in single crystals because the optical path length through the sample is longer in the spectroscopic than in the microscopic measurements. At shorter second harmonic wavelengths, the cocrystals absorb the emitted second harmonic photons, and therefore, SHG signals cannot be detected. This feature, combined with the microscope's higher numerical aperture and the 10^6 faster repetition rate of the microscope laser over that of the laser used for SHG spectroscopy, makes two-photon microscopy, which sacrifices detection range, far more sensitive in detecting second harmonic photons than the laser setup used for spectroscopic measurements. See Experimental Section. As a result, we were able to observe SHG using two-photon microscopy at wavelengths where the cocrystal absorbs a significant fraction of the emitted second harmonic photons.

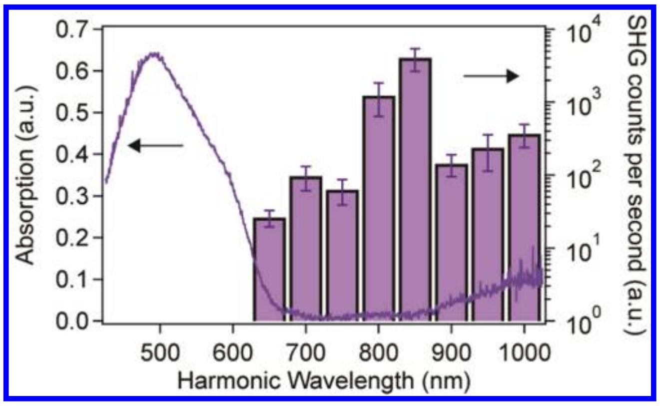

Figure 4. Spectroscopic second harmonic generation (right axis, bar plot) in relation to the optical absorption (left axis, line plot) of the cocrystal $(\mathbf{1})_2{\cdot}\mathbf{2}$. The optical absorption spectrum is adapted from Blackburn et al.[14]

We suggest that there are three possible reasons for observing spontaneous ferroelectric polarization and SHG in the crystallographically centrosymmetric cocrystal $(\mathbf{1})_2{\cdot}\mathbf{2}$. First, hydrogen-bonding interactions play a significant role in the observed spontaneous polarization. The potentially symmetry-breaking hydrogen atoms cannot be located crystallographically because of their weakly diffracting electron shells. Second, space-group averaging of multiple noncentrosymmetric space groups across a crystal has been reported[43] to lead to a centrosymmetric refinement, but this possibility is unlikely given the quality of the X-ray diffraction data obtained. A third explanation for the origin of noncentrosymmetry in cocrystal $(\mathbf{1})_2{\cdot}\mathbf{2}$ could be a result of the asymmetry in the π electron cloud distribution between the donor and acceptor molecules arising from intermolecular charge-transfer interactions.[44−46] In any case, it is clear that the molecular or atomic displacements that break the center of inversion have not been resolved using conventional X-ray crystallography.

Theoretical studies have attempted to predict the remnant polarization and phase transitions in LASO cocrystals. Chen et al.[47] combined density functional theory geometry optimization with polymorph predictors to predict the packing structure and

DOI: 10.1021/jacs.7b02279
J. Am. Chem. Soc. 2017, 139, 9186−9191

spontaneous polarizations obtainable from LASO cocrystals consisting of tetrathiafulvalene donors and pyromellitic diimide-based acceptors. These authors correctly predicted the mixed-stack packing arrangement of the LASO cocrystals,[14] and calculated spontaneous polarizations of up to 127 μC/cm^2. They attribute these high polarizations to the collective contributions of $\pi-\pi$ stacking, charge-transfer, and hydrogen bonding. A different computational study on the ferroelectricity of the LASO cocrystals was carried out by D'Avino et al.[48] using the Peierls−Hubbard model in addition to first-principles calculations. These authors compared the results from their theoretical study to the experimental evidence of ferroelectricity in both LASO as well as other charge-transfer ferroelectric cocrystals.[49,50] Their predictions differed considerably from the experimental data. We believe this difference could be a consequence of an incomplete analysis of the role of hydrogen bonding on the ferroelectric polarization in these charge-transfer complexes. Future theoretical work that takes into account all the noncovalent bonding interactions would help elucidate the origin and mechanism of room-temperature ferroelectricity in these cocrystals.

■ CONCLUSIONS

We have described crystalline alternating stacks of acceptor and donor molecules that exhibit room-temperature ferroelectric behavior along two nearly orthogonal crystallographic axes. We attribute this phenomenon to the combined effects of three-dimensional hydrogen-bonding networks and charge-transfer along more than one axis. These supramolecular materials could offer platforms to design devices with high density and nonvolatile information storage.

■ EXPERIMENTAL SECTION

Purification of Compounds. *N,N'*-Ethoxy(ethanol)-pyromellitic diimide (**1**) was synthesized following previously reported procedures.[8] The solids obtained were dissolved in a minimum volume of hot THF, and the solution was allowed to gradually cool back to room temperature (RT) under ambient conditions. After 6 h, filtration of the crystallization mixture yielded analytically pure **1** as a colorless crystalline powder. A second crop of large, colorless single crystals was obtained after the mother liquor was allowed to stand open to the atmosphere in the filtration flask for several days. Both crops were satisfactory for LASO cocrystallization.

5-Amino-1-naphthol (**2**, Aldrich, 97%) was dissolved in a minimum volume of hot ethanol, and the solution was allowed to gradually cool back to RT under ambient conditions to yield a dark purple solution. The flask containing this solution was placed in a −20 °C fridge overnight to initiate crystallization. Cold filtration of this mixture yielded analytically pure 5-amino-1-naphthol as a dark crystalline powder.

Crystallization of (1)$_2$·2. Recrystallized 5-amino-1-naphthol (13 mg, 82 μmol) was dissolved in a 20 mL scintillation vial containing 11 mL of a 10:1 mixture of 1,2-dichloroethane (Aldrich) and diethyl ether (Aldrich). Subsequently, **1** (17 mg, 43 μmol) was added to the solution, and the mixture was sonicated at 45 °C to fully solubilize **1**. Once this solution was cooled to room temperature, it was passed through a 0.45 μm PTFE syringe filter (Pall Corporation) into a 16 × 150 mm borosilicate test tube (VWR) that was washed with Me$_2$CO and dried in a glassware-drying oven for 3 days prior to use. Next, 10 mL of 1-chlorobutane (Aldrich) was slowly passed through a fresh 0.45 μm PTFE syringe filter and layered carefully on top of the 1,2-dichloroethane mixture. The tube was capped with a rubber septum and allowed to crystallize for 3 days to yield dark purple plate-like crystals that can be several centimeters long and several millimeters wide. The crystals were collected by filtration and washed with *n*-hexane or hexanes prior to being stored in glass vials. Additional notes and observations about the crystallization procedure are provided in the Supporting Information.

Microscopy Measurements. Two-photon confocal microscopy images were obtained using a Nikon A1R MP+ Multiphoton Confocal Microscope, equipped with a Coherent Ti:Sapphire Chameleon Vision S Laser, mode-locked at 80 MHz with a 75 fs pulse duration. The incident laser wavelength was tunable from 690 to 1040 nm. Reflected and transmitted photons were recorded by detectors above and below the sample plane, with detection windows from 380 to 450 nm and 470 to 500 nm. The irradiation power across all incident wavelengths was set at 800 mW. Single crystals of (**1**)$_2$·**2** were sandwiched between a glass microscope slide and coverslip to separate the crystals from the water-immersion microscope objective lens. All samples were irradiated in the dark at room temperature under ambient conditions.

Second Harmonic Generation Experiments. We performed spectroscopic second harmonic generation measurements[51] using a Nd:YAG laser pulsed at 10 Hz with a (54 ± 5) ps pulse duration. This irradiation frequency was tripled (355 nm) and was used to pump a homemade optical parametric amplifier (OPA). A filter passing the longer wavelength was used to remove the signal beam, and the idler beam was focused onto the samples with a 100 mm focal length N-BK7 lens with a spot size on the order of 1 mm. In order to check the SHG efficiency as a function of the excitation energy, we tuned the wavelengths of the idler light from 1100 to 2000 nm. In this range, the spectral bandwidth of the linearly polarized light from the OPA is rather broad, about 2 meV full width at half-maximum. The SHG signal was collected off axis and focused onto a fiber optic bundle. The output of the fiber optic bundle coupled to the entrance slit of an Andor 300i spectrometer and was detected using a DU420-BX2-DD CCD camera. The data-collection time was 10 s.

As-grown crystals of (**1**)$_2$·**2** were crushed and sieved to achieve a size distribution of less than 63 μm. The powdered material was placed into borosilicate capillary tubes (1.5−1.8 mm × 90 mm) and measured at ambient conditions in the dark.

Electronic Measurements. Temperature-dependent dielectric constant and ferroelectric hysteresis measurements were performed on single cocrystals of (**1**)$_2$·**2**. Gold-paste (Ted Pella) electrodes were applied to each cocrystal along either the [100] or [010] axis. Gold wires (12.5 μm diameter) were fixed to the two gold paste contacts and then connected to the ferroelectric tester. All measurements were performed in a He atmosphere within a temperature-controlled Physical Properties Measurement System (PPMS 6000, QuantumDesign).

The dielectric constant was measured using an Agilent E4980A from 8 to 400 K at 2 V at frequencies of 1, 5, or 10 kHz. All ferroelectric measurements were performed with a Radiant Technologies Precision LC, coupled to a Trek Inc. 609A high voltage amplifier.

■ ASSOCIATED CONTENT

Ⓢ Supporting Information

The Supporting Information is available free of charge on the ACS Publications website at DOI: 10.1021/jacs.7b02279.

Details on crystallization, single crystal crystallography and unit cell indexing; additional microscopy, spectroscopy, and electronic measurements for cocrystal (**1**)$_2$·**2** (PDF)

■ AUTHOR INFORMATION

Corresponding Authors

*s-stupp@northwestern.edu
*stoddart@northwestern.edu

ORCID

J. Fraser Stoddart: 0000-0003-3161-3697
Samuel I. Stupp: 0000-0002-5491-7442

Author Contributions

[a]A.N. and D.C. contributed equally.

Notes

The authors declare no competing financial interest.

■ ACKNOWLEDGMENTS

Electrical and imaging measurements performed in the Stupp laboratory were funded by the Office of Science, Office of Basic Energy Sciences, U.S. Department of Energy, under Award No. DE-FG02-00ER45810. Synthesis, crystallization, and X-ray characterization performed in the Stoddart laboratory was funded by the Joint Center of Excellence in Integrated Nano-Systems (JCIN) at King Abdulaziz City for Science and Technology (KACST). D.C. was supported by an NSF Graduate Research Fellowship and a Ryan Fellowship awarded by the International Institute for Nanotechnology (IIN) at Northwestern University (NU). L.F. acknowledges NSF IGERT DGE-0801685 and the Institute for Sustainability and Energy at Northwestern (ISEN). A.K.B. acknowledges a Fulbright Graduate Award and a New Zealand Federation of Graduate Women Postgraduate Fellowship Award. Imaging work was performed at the NU Center for Advanced Microscopy and was supported by NCI CCSG P30 CA060553, awarded to the Robert H. Lurie Comprehensive Cancer Center. Multiphoton microscopy was performed on a Nikon A1R multiphoton microscope, acquired through the support of NIH 1S10OD010398-01. Spectroscopic nonlinear optical and electrical measurements were performed at the Magnet, Low Temperature, and Optical Facility supported by the NSF's MRSEC program (DMR-1121262) at the Materials Research Center of NU.

■ REFERENCES

(1) Scott, J. F.; Paz de Araujo, C. A. *Science* **1989**, *246*, 1400−1405.

(2) Scott, J. F. *Science* **2007**, *315*, 954−959.

(3) Rabe, K. M., Ahn, C. H., Triscone, J.-M., Eds.; *Physics of Ferroelectrics: A Modern Perspective*; Springer: Berlin; New York, 2007.

(4) Lines, M. E.; Glass, A. M. *Principles and Applications of Ferroelectrics and Related Materials*; Oxford University Press: New York, 2001.

(5) Miller, R. C. *Phys. Rev.* **1964**, *134*, A1313−A1319.

(6) Frey, M. H.; Payne, D. A. *Phys. Rev. B: Condens. Matter Mater. Phys.* **1996**, *54*, 3158−3168.

(7) Tayi, A. S.; Kaeser, A.; Matsumoto, M.; Aida, T.; Stupp, S. I. *Nat. Chem.* **2015**, *7*, 281−294.

(8) Tayi, A. S.; Shveyd, A. K.; Sue, A. C.-H.; Szarko, J. M.; Rolczynski, B. S.; Cao, D.; Kennedy, T. J.; Sarjeant, A. A.; Stern, C. L.; Paxton, W. F.; Wu, W.; Dey, S. K.; Fahrenbach, A. C.; Guest, J. R.; Mohseni, H.; Chen, L. X.; Wang, K. L.; Stoddart, J. F.; Stupp, S. I. *Nature* **2012**, *488*, 485−489.

(9) Horiuchi, S.; Tokura, Y. *Nat. Mater.* **2008**, *7*, 357−366.

(10) Fu, D.-W.; Cai, H.-L.; Liu, Y.; Ye, Q.; Zhang, W.; Zhang, Y.; Chen, X.-Y.; Giovannetti, G.; Capone, M.; Li, J.; Xiong, R.-G. *Science* **2013**, *339*, 425−428.

(11) Stupp, S. I.; Palmer, L. C. *Chem. Mater.* **2014**, *26*, 507−518.

(12) Foster, R. *Organic Charge-Transfer Complexes*, 2nd ed.; Academic Press: London, 1970.

(13) Torrance, J. B.; Vazquez, J. E.; Mayerle, J. J.; Lee, V. Y. *Phys. Rev. Lett.* **1981**, *46*, 253−257.

(14) Blackburn, A. K.; Sue, A. C.-H.; Shveyd, A. K.; Cao, D.; Tayi, A. S.; Narayanan, A.; Rolczynski, B. S.; Szarko, J. M.; Bozdemir, O. A.; Wakabayashi, R.; Lehrman, J. A.; Kahr, B.; Chen, L. X.; Nassar, M. S.; Stupp, S. I.; Stoddart, J. F. *J. Am. Chem. Soc.* **2014**, *136*, 17224−17235.

(15) Dawber, M.; Chandra, P.; Littlewood, P. B.; Scott, J. F. *J. Phys.: Condens. Matter* **2003**, *15*, L393.

(16) Mehta, R. R.; Silverman, B. D.; Jacobs, J. T. *J. Appl. Phys.* **1973**, *44*, 3379.

(17) Scott, J. F. *J. Phys.: Condens. Matter* **2008**, *20*, 21001.

(18) Naumov, I. I.; Bellaiche, L.; Fu, H. *Nature* **2004**, *432*, 737−740.

(19) McQuaid, R. G. P.; McGilly, L. J.; Sharma, P.; Gruverman, A.; Gregg, J. M. *Nat. Commun.* **2011**, *2*, 404.

(20) Rodriguez, B. J.; Gao, X. S.; Liu, L. F.; Lee, W.; Naumov, I. I.; Bratkovsky, A. M.; Hesse, D.; Alexe, M. *Nano Lett.* **2009**, *9*, 1127−1131.

(21) Gruverman, A.; Wu, D.; Fan, H.-J.; Vrejoiu, I.; Alexe, M.; Harrison, R. J.; Scott, J. F. *J. Phys.: Condens. Matter* **2008**, *20*, 342201.

(22) Jia, C.-L.; Urban, K. W.; Alexe, M.; Hesse, D.; Vrejoiu, I. *Science* **2011**, *331*, 1420−1423.

(23) Balke, N.; Winchester, B.; Ren, W.; Chu, Y. H.; Morozovska, A. N.; Eliseev, E. A.; Huijben, M.; Vasudevan, R. K.; Maksymovych, P.; Britson, J.; Jesse, S.; Kornev, I.; Ramesh, R.; Bellaiche, L.; Chen, L. Q.; Kalinin, S. V. *Nat. Phys.* **2011**, *8*, 81−88.

(24) Horiuchi, S.; Kagawa, F.; Hatahara, K.; Kobayashi, K.; Kumai, R.; Murakami, Y.; Tokura, Y. *Nat. Commun.* **2012**, *3*, 1308.

(25) Lutkenhaus, J. L.; McEnnis, K.; Serghei, A.; Russell, T. P. *Macromolecules* **2010**, *43*, 3844−3850.

(26) Lovinger, A. J.; Davis, D. D.; Cais, R. E.; Kometani, J. M. *Macromolecules* **1986**, *19*, 1491−1494.

(27) Koga, K.; Ohigashi, H. *J. Appl. Phys.* **1986**, *59*, 2142−2150.

(28) Schein, B. J. B.; Lingafelter, E. C.; Stewart, J. M. *J. Chem. Phys.* **1967**, *47*, 5183−5189.

(29) Tokura, Y.; Koshihara, S.; Iwasa, Y.; Okamoto, H.; Komatsu, T.; Koda, T.; Iwasawa, N.; Saito, G. *Phys. Rev. Lett.* **1989**, *63*, 2405.

(30) Kagawa, F.; Minami, N.; Horiuchi, S.; Tokura, Y. *Nat. Commun.* **2016**, *7*, 10675.

(31) Westrip, S. P. *J. Appl. Crystallogr.* **2010**, *43*, 920−925.

(32) Spek, A. L. *Acta Crystallogr., Sect. D: Biol. Crystallogr.* **2009**, *65*, 148−155.

(33) Fiebig, M.; Pavlov, V. V.; Pisarev, R. V. *J. Opt. Soc. Am. B* **2005**, *22*, 96−118.

(34) Ok, K. M.; Chi, E. O.; Halasyamani, P. S. *Chem. Soc. Rev.* **2006**, *35*, 710−717.

(35) Coda, A.; Pandarese, F. *J. Appl. Crystallogr.* **1976**, *9*, 193−198.

(36) Nalla, V.; Medishetty, R.; Wang, Y.; Bai, Z.; Sun, H.; Wei, J.; Vittal, J. J. *IUCrJ* **2015**, *2*, 317−321.

(37) Patil, P. S.; Bhumannavar, V. M.; Bannur, M. S.; Kulkarni, H. N.; Bhagavannarayana, G. *J. Cryst. Process Technol.* **2013**, *3*, 108−117.

(38) Cai, H.-L.; Fu, D.-W.; Zhang, Y.; Zhang, W.; Xiong, R.-G. *Phys. Rev. Lett.* **2012**, *109*, 16901.

(39) Shi, P.-P.; Tang, Y.-Y.; Li, P.-F.; Liao, W.-Q.; Wang, Z.-X.; Ye, Q.; Xiong, R.-G. *Chem. Soc. Rev.* **2016**, *45*, 3811−3827.

(40) Campagnola, P. J.; Loew, L. M. *Nat. Biotechnol.* **2003**, *21*, 1356−1360.

(41) Bergman, J. G.; McFee, J. H.; Crane, G. R. *Appl. Phys. Lett.* **1971**, *18*, 203−205.

(42) Jain, P.; Stroppa, A.; Nabok, D.; Marino, A.; Rubano, A.; Paparo, D.; Matsubara, M.; Nakotte, H.; Fiebig, M.; Picozzi, S.; et al. *Quantum Mater.* **2016**, *1*, 16012.

(43) Desiraju, G. R.; Curtin, D. Y.; Paul, I. C. *Mol. Cryst. Liq. Cryst.* **1979**, *52*, 259−266.

(44) Sipe, J. E.; Moss, D. J.; van Driel, H. M. *Phys. Rev. B: Condens. Matter Mater. Phys.* **1987**, *35*, 1129−1141.

(45) Dadap, J. I.; Shan, J.; Heinz, T. F. *J. Opt. Soc. Am. B* **2004**, *21*, 1328−1347.

(46) Guo, W.; Guo, F.; Wei, C.; Liu, Q.; Zhou, G.; Wang, D.; Shao, Z. *Sci. China Ser. B Chem.* **2002**, *45*, 267−274.

(47) Chen, S.; Zeng, X. C. *J. Am. Chem. Soc.* **2014**, *136*, 6428−6436.

(48) D'Avino, G.; Verstraete, M. J. *Phys. Rev. Lett.* **2014**, *113*, 237602.

(49) Horiuchi, S.; Okimoto, Y.; Kumai, R.; Tokura, Y. *J. Phys. Soc. Jpn.* **2000**, *69*, 1302−1305.

(50) Torrance, J. B.; Girlando, A.; Mayerle, J. J.; Crowley, J. I.; Lee, V. Y.; Batail, P.; LaPlaca, S. J. *Phys. Rev. Lett.* **1981**, *47*, 1747.

(51) Kurtz, S. K.; Perry, T. T. *J. Appl. Phys.* **1968**, *39*, 3798−3813.